We are IntechOpen,
the world's leading publisher of Open Access books
Built by scientists, for scientists

6,900
Open access books available

186,000
International authors and editors

200M
Downloads

154
Countries delivered to

Our authors are among the

TOP 1%
most cited scientists

12.2%
Contributors from top 500 universities

CLARIVATE ANALYTICS
BOOK CITATION INDEX
INDEXED

WEB OF SCIENCE™

Selection of our books indexed in the Book Citation Index
in Web of Science™ Core Collection (BKCI)

Interested in publishing with us?
Contact book.department@intechopen.com

Numbers displayed above are based on latest data collected.
For more information visit www.intechopen.com

Recent Advances in Visible-Light Driven Photocatalysis

Yuhua Wang, Xinlong Ma, Hao Li, Bin Liu, Huihui Li, Shu Yin and Tsugio Sato

Additional information is available at the end of the chapter

Abstract

Semiconductor photocatalysis has been considered a potentially promising approach for renewable energy and environmental remediation with abundant solar light. However, the currently available semiconductor materials are generally limited by either the harvesting of solar energy or insufficient charge separation ability. To overcome the serious drawbacks of narrow light-response range and low efficiency in most photocatalysts, many strategies have been developed in the past decades. This article reviews the recent advancements of visible-light-driven photocatalysts and attempts to provide a comprehensive update of some strategies to improve the efficiency, such as doping, coupling with graphene, precipitating with metal particles, crystal growth design, and heterostructuring. A brief introduction to photocatalysts is given first, followed by an explanation of the basic rules and mechanisms of photocatalysts. This chapter focuses on recent progress in exploring new strategies to design TiO_2-based photocatalysts that aim to extend the light absorption of TiO_2 from UV wavelengths into the visible region. Subsequently, some strategies are also used to endow visible-light-driven Ag_3PO_4 with high activity in photocatalytic reactions. Next, a novel approach, using long afterglow phosphor, has been used to associate a fluorescence-emitting support to continue the photocatalytic reaction after turning off the light. The last section proposes some challenges to design high efficiency of photocatalytic systems.

Keywords: Photocatalysts, TiO_2, Ag_3PO_4, graphene, long afterglow phosphor

1. Introduction

It is well known that environmental pollution is affecting human survival and development. Photocatalytic technology is considered as an efficient, stable, and environmentally friendly method in the field of environmental pollution control [1]. In general, a photocatalytic reaction includes three steps [2] (Fig. 1). First, electrons (e−) and holes (h+) are generated through

photoexcitation. Then, these electrons and holes migrate to the surface of photocatalysts and subsequently react with adsorbed electron acceptors and donors, respectively. Thus, an efficient photocatalyst requires a semiconductor with a suitable band gap for harvesting light, facile separation and transportation of charge carriers, and proper valence band (VB) and conduction band (CB) edge potential for redox reaction being feasible. To date, much effort is currently focused on how to improve the light absorption, charge separation, and surface reactivity in order to achieve outstanding photocatalytic performance, such as doping, coupled with graphene, precipitated with metal particles, crystal growth design, and heterostructuring.

In the past few decades, TiO_2 nanomaterials have attracted tremendous interest in environmental pollution removal and photocatalytic hydrogen generation. However, all of them have large electronic band gaps of 3.0–3.2 eV, which means only less than 5% of the entire solar energy can be utilized. Thus, much effort has been devoted to bring about the absorption of TiO_2 into the visible-light region and improved photocatalytic activity.
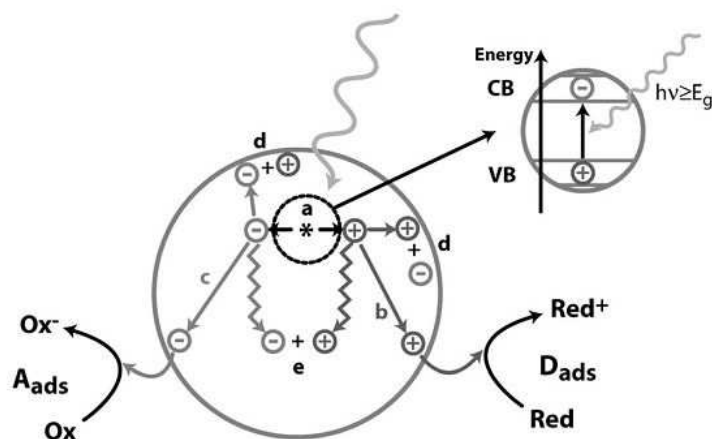

Figure 1. Schematic illustration of the reactions following light absorption by a photocatalyst. (a) Electron–hole pair formation; (b) donor oxidation by hole; (c) reduction by electron; (d) and (e) electron–hole recombination on the surface or in the bulk. Adapted with permission from ref. 2. © 1995 ACS.

Despite the fact that there are many research articles on modified TiO_2, the exploration of new active and efficient visible-light-driven photocatalysts attracts much attention [3–22]. In the effort to exploit novel photocatalyst systems working under visible light, it has been revealed that orbitals of some p-block metals with a d10 configuration [22], such as Ag 4d in Ag(I), could hybridize O 2p levels to form a new preferable hybridized VB, thus narrowing the band gap to harvest visible light.

Compared with single-phase semiconductor photocatalysts, hybrids of two or more semiconductor systems, i.e., heterostructures, seem to possess advantages in more efficiently utilizing solar light. Besides metal/semiconductor and carbon group materials/semiconductor-heterostructured photocatalysts [23–28], semiconductor/semiconductor-heterostructured photocatalysts with diverse models have been developed (Fig. 2), including type-I and type-II heterojunctions, Z-scheme, p–n heterojunctions, and homojunction band alignments [29–32].

Figure 2. Schematic illustration of band alignments corresponding to five kinds of heterostructured photocatalysts, including the straddling alignment (type I), staggered alignment (type II), Z-scheme system, p–n heterojunctions, and homojunctions. Reproduced with permission from ref. 30–32 © 2011 RSC & 2011 ACS & 2012 Wiley.

2. TiO$_2$-based photocatalysts

In this section, strategies on the modulation of energy band structures or surface states of wide-band-gap photocatalysts, especially for TiO$_2$, are reviewed. Currently, many strategies have been developed to modulate the band structures of TiO$_2$, including doping, coupling with graphene, precipitating with metal particles, crystal growth design, and heterostructuring, which will be discussed.

2.1. Doping

Doping is an available strategy to tune the absorption band of wide-band photocatalysts. Several studies have investigated nonmetal doping. Asahi *et al.* reported nitrogen-doped TiO$_2$ of nonmetals, such as N [33, 34], C [35–37], S [38, 39], B [40–42], F [43–45], Br [46], I [47–50], P [51], in 2001 [33]. In our study [34], nitrogen-doped titania nanoparticles (NPs) were successfully prepared by a microwave-assisted solvothermal process in a very short time, and the prepared samples showed visible-light absorption in the range of 400–550 nm, indicating its potential applications as visible-light-induced photocatalyst. The chemical states and locations of dopants are considered to be key factors in adjusting the spectral distribution of

the induced electronic states of those dopants and reconstructing favorable surface structure for photocatalysis.

Co-doping with two suitable heteroatoms can also achieve substantial synergistic effects [41, 52–55]. For example, B, N co-doped TiO_2, benefits from the B–N bonds formed, which can increase the amount of doped N on the TiO_2 surface and the promoted separation of photo-excited electron–hole pairs [41].

2.2. TiO_2-graphene composite

Graphene, a two-dimensional carbonaceous material, can be used in many applications due to its unique and remarkable properties such as high conductivity, large surface area, and good chemical stability [56–59]. Tremendous interest is devoted to fabricating numerous graphene–semiconductor composites to aid charge separation and migration and improve the performance of the photocatalysts [60–64]. Graphene works as an electron acceptor or transporter to induce electron transfer, leading to an efficient charge separation. Thus, an appropriate integration of graphene and TiO_2 could give rise to a nanocomposite that combines the desirable properties of graphene and TiO_2, e.g., the photocatalytic activity of TiO_2 can be improved. In the past few years, there were some reports about graphene–TiO_2 composites [13–17].

Recently, Liu et al. synthesized the graphene oxide–TiO_2 nanorod composites [65, 66]. Wu et al. reported the synthesis and application of graphene–TiO_2 nanorod hybrid nanostructures in microcapacitors [67]. As shown in Fig. 3, the assembling of TiO_2 nanocrystalline with exposed {001} facets on graphene sheets reported in our previous work showed a higher photocatalytic activity than the other normal TiO_2/graphene composites [68]. In another work (Fig. 4), graphene/rod-shaped TiO_2 nanocomposite was synthesized by the solvothermal method [69]. In a one-pot system, the rod-shaped TiO_2 can be homogeneously dispersed on the surface of graphene sheets by syngraphenization strategy. Owing to the combination of graphene and rod-shaped TiO_2, the graphene/rod-shaped TiO_2 nanocomposite shows a significant enhancement in the photocatalytic performance compared with that of the graphene/spherical TiO_2 nanocomposite, which can be attributed to the high electronic mobility of graphene, higher Brunauer-Emmett-Teller (BET) surface area, and rod-shaped structures of TiO_2. In our recent work [70], a series of B-doped graphene/rod-shaped TiO_2 nanocomposites were synthesized via one-step hydrothermal reaction. The photocatalytic activity of the obtained nanocomposites for the oxidative photodestruction of NO*x* gas showed better photocatalytic properties than pure TiO_2 and graphene/TiO_2 nanocomposites. This work provides new insight into the fabrication of TiO_2–carbon nanocomposites as high-performance photocatalysts and facilitates their application in addressing environmental protection issues.

2.3. TiO_2-based plasmonic photocatalysts

Plasmonic photocatalysis has offered a new opportunity to solve the problem of the limited efficiency of photocatalysts [71–73]. In these photocatalysts, the nanostructured plasmonic metals are often combined with a semiconductor-based material (e.g., TiO_2), and the photo-catalytic activity is greatly enhanced due to the local surface plasmon resonance (LSPR) effect
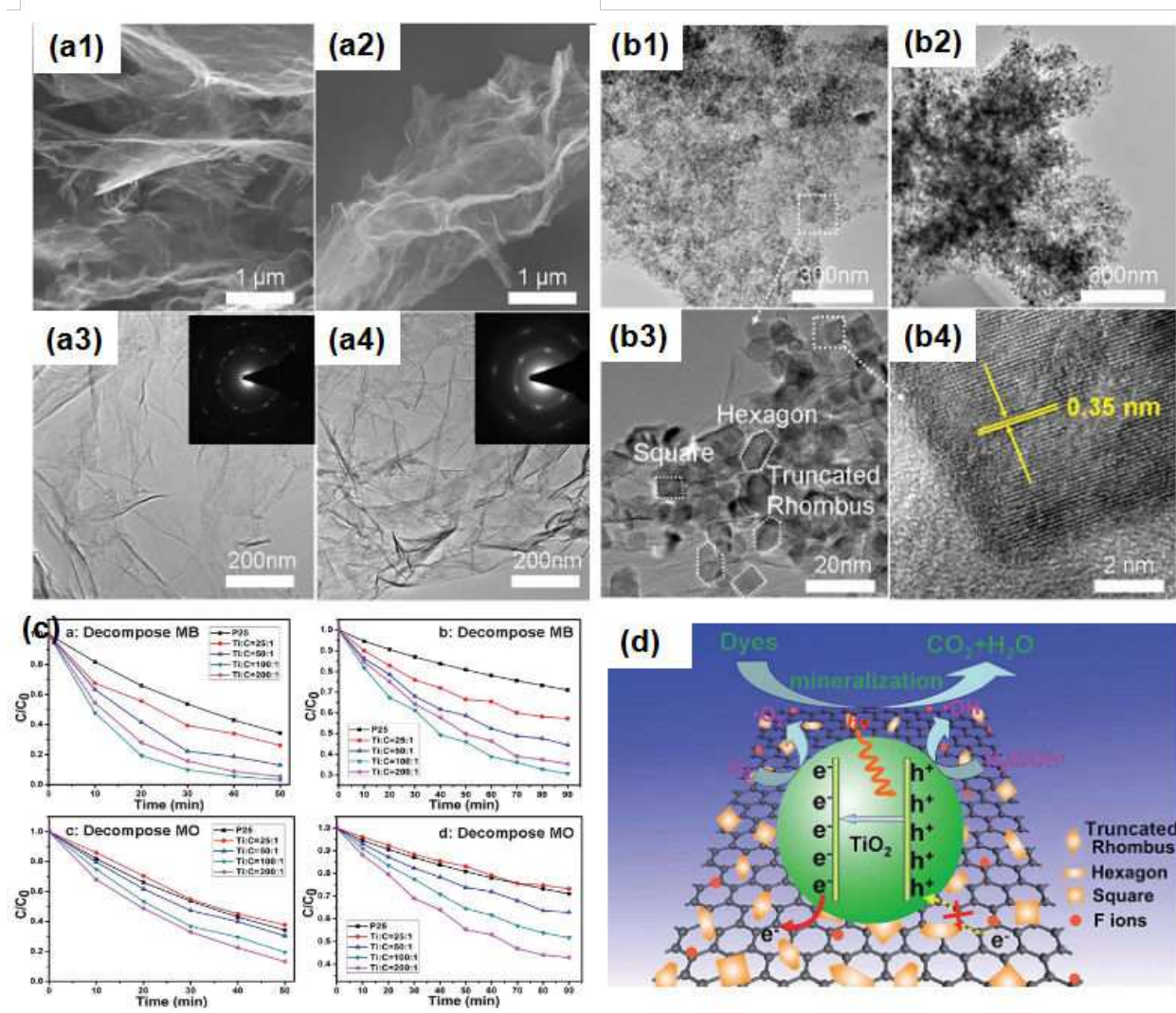
Figure 3. Scanning electron micrograph (SEM) and transmission electron micrograph (TEM) of (a1 and a3) GO and (a2 and a4) GS; (b1 and b2) TEM images of TiO_2/GS with different Ti:C ratios; (b3 and b4) high-resolution transmission electron microscopic (HRTEM) images of sample b1; (c) photocatalytic degradation of MB and MO under the irradiation of UV light and visible light over the TiO_2/GS composites; (d) a proposed schematic illustration showing the reaction mechanism for photocatalytic degradation of organic pollutants over the TiO_2/GS composites. Reproduced with permission from ref. 68 © 2012 RSC.

[74]. The LSPR effect endows the metal nanocrystals with very large absorption and scattering cross sections and local electromagnetic field enhancement in the near-field region near the surface of plasmonic metal nanocrystals, which is promising in manipulating light absorption in photocatalytic systems. The intensity of the local electromagnetic field is several orders of magnitude larger than that of the far-field incident light, and the highest charge carrier formation is observed at the semiconductor/liquid interface, which benefits the photocatalytic reactions [71–72].

Recently, noble metal nanoparticle-deposited TiO_2 has attracted significant attention. The main advantages of these noble metal NPs can be attributed to their chemically inert properties
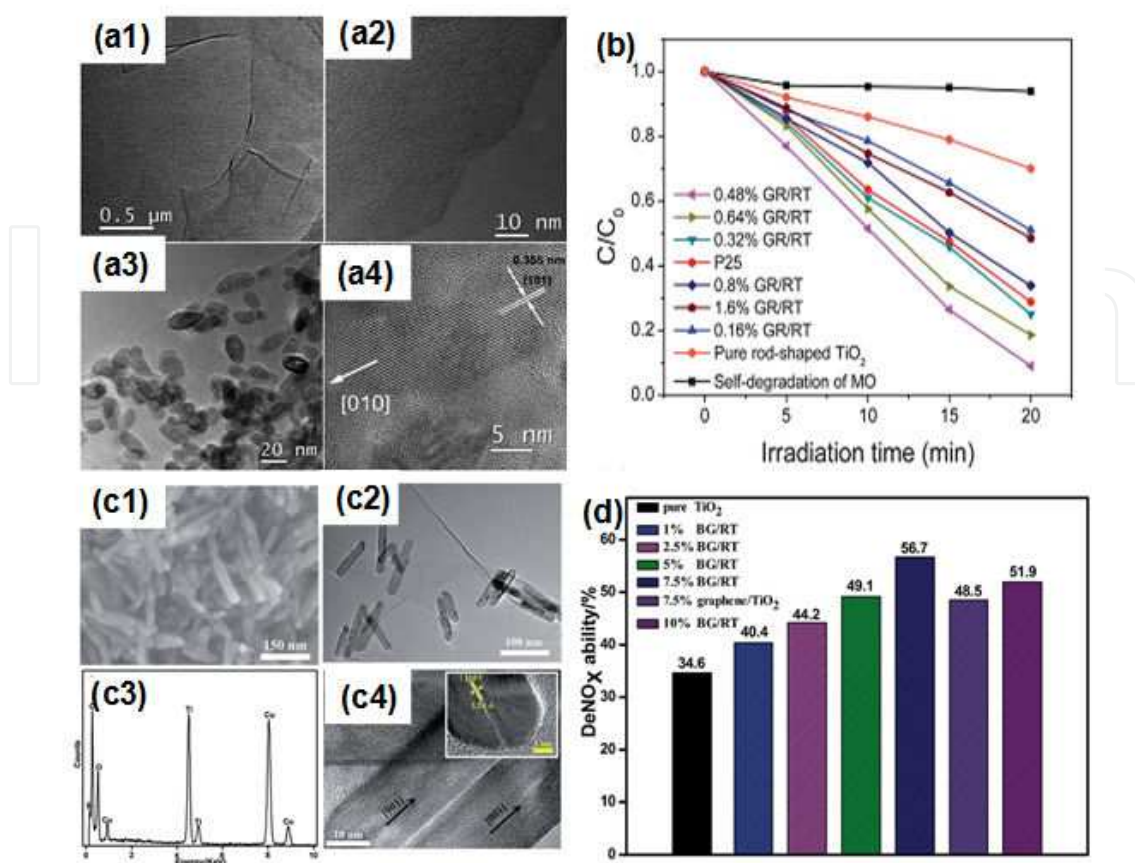
Figure 4. TEM images of (a1) graphene oxide, (a2) graphene, (a3) 0.48% GR/RT, and (a4) HRTEM image of a single rod-shaped TiO_2 nanocrystal in the composite; (b) photocatalytic degradation of MO solution over graphene/rod-shaped TiO_2 nanocomposites with various graphene contents compared with that of GR/ST; (c1) SEM image, (c2) TEM image, (c3) EDX, and (c4) HRTEM image of 7.5% BG/RT; (d) photocatalytic activity for the destruction of NOx gas under UV irradiation using different photocatalysts. Reproduced with permission from ref. 69 & ref. 70 © 2012 & 2014 RSC.

toward (photo) oxidation and LSPR effect on the surface [75, 76]. Meanwhile, our previous work found the plasmonic enhancement of the photocatalytic activity of semiconductor–metal nanocomposite materials [77–79]. Thus, noble metal NP-deposited TiO_2 could be an appropriate approach to improve the photocatalytic performance of TiO_2.

A variety of nanostructured Au/TiO_2 with different morphologies have been synthesized, such as highly stable mesoporous Au/TiO_2 spheres (~500 nm) [80] and mesoporous Au–TiO_2 nanocomposites using a simple spray hydrolytic method [81]. In our study, Au NPs are precipitated on the highly porous one-dimensional (1D) TiO_2 nanotubes (NTs), and the plasmonic photocatalytic properties of the material are investigated [82]. Compared with nanoparticles, there are some advantages of 1D NT structures, such as favorable recycling characteristics and the vectorial transport of photogenerated charge carriers [83, 84], which have great potential for superior photocatalytic performance. The Au NPs/TiO_2 NTs were synthesized by emulsion electrospinning followed by deposition–precipitation (DP) method. The results in Fig. 5 show that the modified porous TiO_2 NTs with the presence of Au NPs increased photocatalytic destruction of methylene blue (MB) solution under visible-light irradiation. Furthermore, the migration of Au NPs from the rutile phase to the interface of

rutile/anatase was found when the calcination temperature changed from 250 °C to 350 °C. The optimal photocatalytic activity was obtained in the sample $Au_3(DP_{350})/TiO_2$, due to the plasmon activation of the Au NPs followed by consecutive electron transfer that induced efficient charge separation. Therefore, such a highly porous Au/TiO_2 heterojunction structure provides a new pathway for the design and fabrication of other energy- and environment-related applications.
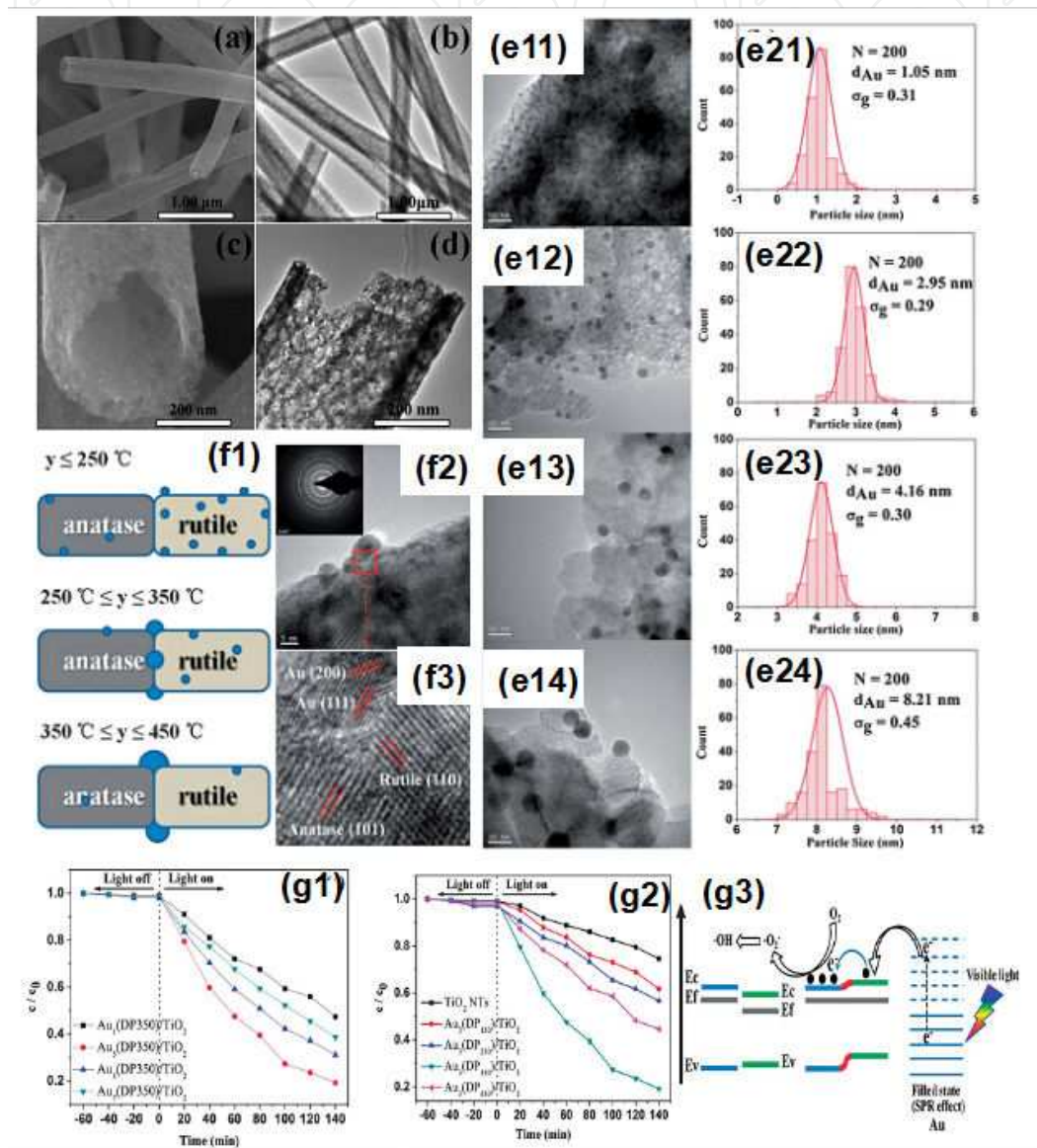

Figure 5. (a) SEM and (b) TEM images of as-prepared TiO_2 NTs and (c) SEM and (d) TEM images of the representative sample $Au_3(DP_{350})/TiO_2$ NTs; TEM images of $Au_3(DP_y)/TiO_2$ (y = 150 (e11), 250 (e12), 350 (e13), and 450 °C (e14), respectively) and the dispersion of Au co-catalysts (e21), (e22), (e23), and (e24), respectively; (f1) effect of calcination temperature on the location and size of the Au NPs on TiO_2 NTs; (f2 and f3) TEM and HRTEM images of $Au_3(DP_{350})/TiO_2$. Variation of normalized C/C_0 of MB concentration as a function of visible-light irradiation time for (g1) $Au_x(DP_{350})/TiO_y$ and (g2) $Au_3(DP_y)/TiO_2$ (y = 150, 250, 350, 450 °C, respectively); (g3) schematic diagram for the possible mechanism for photocatalytic degradation of MB over $Au_3(DP_{350})/TiO_2$ under visible-light irradiation. Reproduced with permission from ref. 82 © 2013 RSC.

2.4. TiO$_2$-based heterostructure photocatalysts

The heterojunctions provide a facile way to enable the effective separation of photoexcited electron–hole pairs, thus to enhance the photocatalytic performance. Table 1 lists recent prominent heterostructured photocatalysts as well as their photocatalytic application.

	Heterostructured photocatalysts
Type I	CdS/ZnS,[85] Bi2S3/CdS,[86] V$_2$O$_5$/BiVO$_4$[30]
Type II	CdS/TiO$_2$,[87–89] SrTiO$_3$/TiO$_2$,[90, 91] Fe$_2$O$_3$/TiO$_2$,[92] ZnO/CdS,[93] AgIn5S8/TiO$_2$,[94] Ag$_3$VO$_4$/TiO$_2$[95] ZnFe$_2$O$_4$/TiO$_2$[96]
p–n	CuFe$_2$O$_4$/TiO$_2$,[97] CuO/ZnO,[98] MoS2/CdS,[99, X] Ag$_2$O/TiO$_2$,[101] CuInSe$_2$/TiO$_2$,[102] TiO$_2$/ZnO,[103] ZnFe$_2$O$_4$/TiO$_2$,[104] NiO/ZnO[105]
Homojunction	Anatase/rutile TiO$_2$,[106] α/β-Ga2O3,[31] p–n Cu2O,[107] α/γ-Bi$_2$O$_3$,[108] Co-doped TiO$_2$/TiO$_2$,[109] W-doped BiVO$_4$,[110] Pt/n-Si/n+-Si/Ag[111]
Z-scheme	CdS/Au/TiO1.96C0.04,[112] CdS/Au/TiO$_2$,[113] ZnO/CdS,[114] CdS/Au/ZnO,[115] CuO/TiO$_2$,[116] CaFe$_2$O$_4$/WO$_4$[117]

Table 1. Recent reports of diverse heterostructured photocatalysts.

According to different electronic energy levels and band gaps of photocatalysts, five kinds of semiconductor heterojunctions have been reported: straddling alignment (type I), staggered alignment (type II), Z-scheme system, homojunctions, and p–n heterojunctions [118, 119]. In those work, the dynamics of electron and hole were studied, including the band gap, the electron affinity, and the work function of different semiconductor heterojunctions.

3. Visible-light-driven Ag$_3$PO$_4$ photocatalysts

A breakthrough was made in finding a novel semiconductor material, Ag$_3$PO$_4$, as an active visible-light-induced photocatalyst [4]. Ag$_3$PO$_4$ demonstrates extremely high capability for O$_2$ evolution from H$_2$O and organic dye decomposition under visible-light irradiation [120]. More importantly, this novel photocatalyst can achieve a quantum efficiency up to 90% at wavelengths longer than 420 nm, which is clearly higher than that reported previously by using semiconductor photocatalysis.

So far, various methods have been proposed to further enhance the photocatalytic activity of Ag$_3$PO$_4$ under visible-light irradiation. One approach is the synthesis of Ag$_3$PO$_4$ with various morphologies. This is because photocatalytic reactions are typically surface-based processes; thus, the photocatalytic efficiency is closely related to the morphology and microstructure of a photocatalyst [83]. Recently, some new morphologies of Ag$_3$PO$_4$ have been developed [120–126]. For example, Bi et al. fabricated the single-crystalline Ag$_3$PO$_4$ rhombic dodecahedrons and cubes, and they found that both of these samples exhibited higher photocatalytic activity

than the microsized spherical Ag_3PO_4 particles [120]. Liang et al. synthesized hierarchical Ag_3PO_4 porous microcubes with enhanced photocatalytic property [123]. Wang et al. reported the synthesis of Ag_3PO_4 tetrapod microcrystals, and they demonstrated that Ag_3PO_4 tetrapod showed higher photocatalytic activity than the microsized spherical Ag_3PO_4 particles [126].

Another approach is to couple Ag_3PO_4 with other semiconductors, carbon materials, or noble metals to improve the photocatalytic activity, such as Ag_3PO_4/TiO_2 [127, 128], Ag_3PO_4/AgX (X = Cl, Br, I) [129], $Ag_3PO_4/BiOCl$ [130], Ag_3PO_4/Fe_3O4 [131], Ag_3PO_4/SnO_2 [132], $Ag_3PO_4/$ carbon quantum dots [133], $Ag_3PO_4/$reduced graphite oxide sheets [134], and Ag_3PO_4/Ag composites [135–137].

3.1. Crystal growth design

Manipulating the crystal structure will result in controlling the percentage of exposed facets on crystal surfaces and thus can lead to a dramatic change in reactivity, which has been widely investigated in sensing [138], electronics [139], magnetic memory devices [140], and catalysis [141]. It is widely accepted in catalysis that a higher surface energy leads to a more reactive surface. Therefore, the control of the exposed facets is one of the most available and efficient methods to obtain more active surface [142], which has been investigated recently to promote photocatalytic activity [83].

Herein, we controllably prepared Ag_3PO_4 crystals with various new morphologies (including branched, tetrapod, nanorod-shaped, and triangular-prism-shaped Ag_3PO_4 crystals) via a facile and efficient synthesis process in the solvent mixture of N,N dimethylformamide (DMF) and H_2O at room temperature (Fig. 6). The results indicate that the branched Ag_3PO_4 sample shows highly enhanced photocatalytic activity compared with other as-prepared Ag_3PO_4 samples, and the BET-specific surface area makes a greater contribution to the enhanced photocatalytic activity of as-prepared Ag_3PO_4 crystals [143].

3.2. Ag_3PO_4–graphene composite

The photocorrosion phenomenon of Ag_3PO_4 reduces the photocatalytic activity during the process. Up to now, some solutions have been put forward to improve its stability and photocatalytic properties under visible-light irradiation. Apart from its unique electronic properties [58], graphene has several other excellent attributes, such as the large theoretical specific surface area [57] and good chemical stability [59]. The large specific surface area of graphene facilitates the attachment of inorganic nanomaterials [144, 145]. Thus, the combination of graphene and Ag_3PO_4 could be a good choice to construct a stable and efficient photocatalyst composite.

In one of our works, Ag_3PO_4/reduced graphite oxide (RGO) nanocomposites were synthesized to enhance the visible-light photocatalytic activity and the stability of Ag_3PO_4. The results show that the graphene content obviously affects the photocatalytic activity of Ag_3PO_4/RGO nanocomposites [134]. As shown in Fig. 7, among a series of Ag_3PO_4/RGO, the Ag_3PO_4/2.1 wt % RGO shows the best photocatalytic activity despite the degradation of MB or Methyl Orange (MO) solution. In addition, the Ag_3PO_4/RGO is more stable than pure Ag_3PO_4 since the RGO
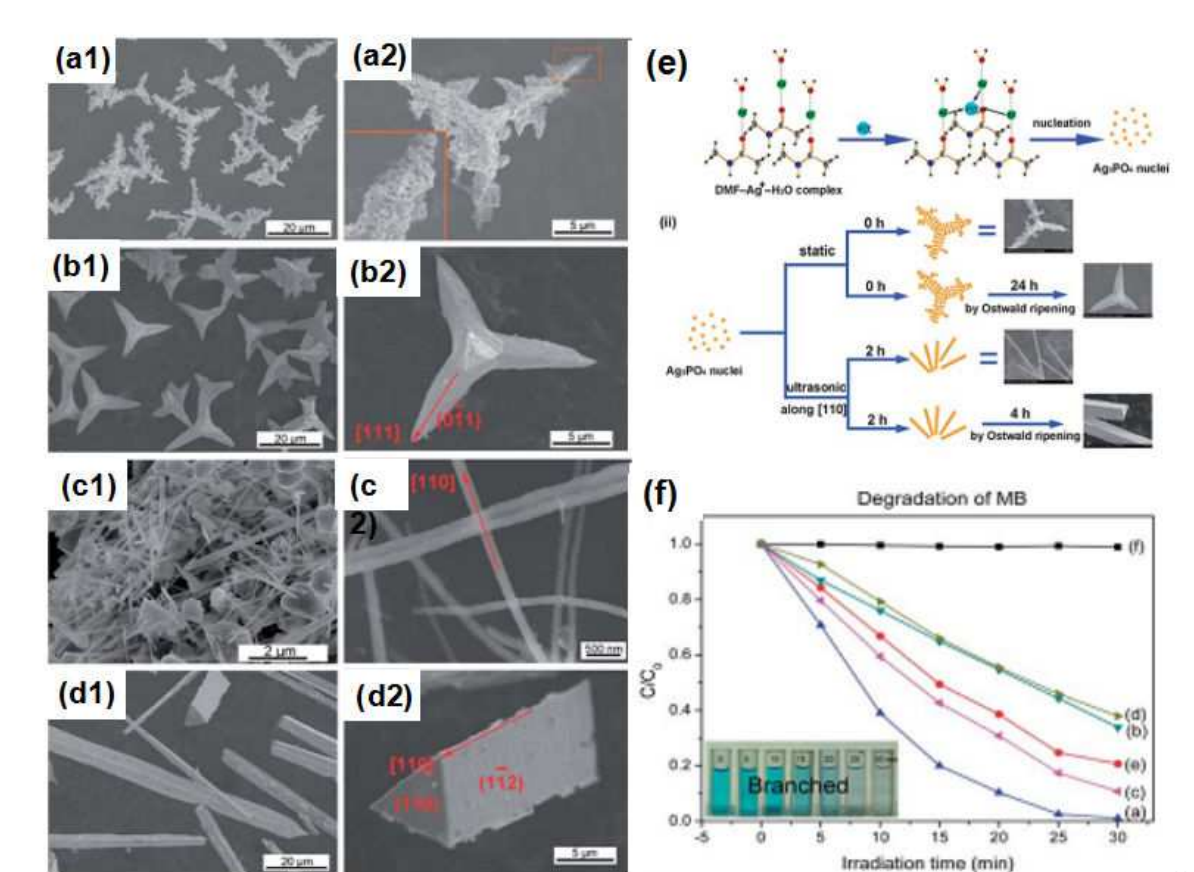
Figure 6. SEM images of (a) branched, (b) tetrapod, (c) nanorod-shaped, and (d) triangular-prism-shaped Ag_3PO_4 crystals; (e) schematic illustration of the possible formation mechanism of Ag_3PO_4 crystals with four typical morphologies prepared under static and ultrasonic conditions; (f) variation of MB solution concentration against illumination time in the presence of branched, tetrapod, nanorod-shaped, triangular-prism-shaped, and irregular spherical Ag_3PO_4 products. Reproduced with permission from ref. 143 © 2013 RSC.

can be used as protective coatings that inhibit the photocorrosion of Ag_3PO_4. Thus, the Ag_3PO_4/RGO nanocomposites with excellent photocatalytic performance and enhanced stability can find promising applications in addressing environmental protection issues.

3.3. Ag_3PO_4-based heterostructure photocatalysts

Many narrow-band-gap metal oxides or chalcogenides have been coupled with Ag_3PO_4 photocatalyst to enhance its photocatalytic activity and/or improve its stability. In Yao's work, Ag_3PO_4/TiO_2 has been synthesized via the in situ deposition of Ag_3PO_4 nanoparticles onto the TiO_2 surface, which facilitates electron–hole separation, thereby leading to enhanced photocatalytic activity [128].

In our work, the phenomenon of "self-corrosion" was first observed in the simple physical mixed Ag_3PO_4/TiO_2 compounds (Fig. 8). It is found that both self-corrosion and photocorrosion in Ag_3PO_4/TiO_2 compounds alter the chemical environment of Ag. The corrosion degree, however, is different due to a slight difference in the chemical environment of Ag. Furthermore, it is the strong adsorption capacity that determines the photocatalytic activities of
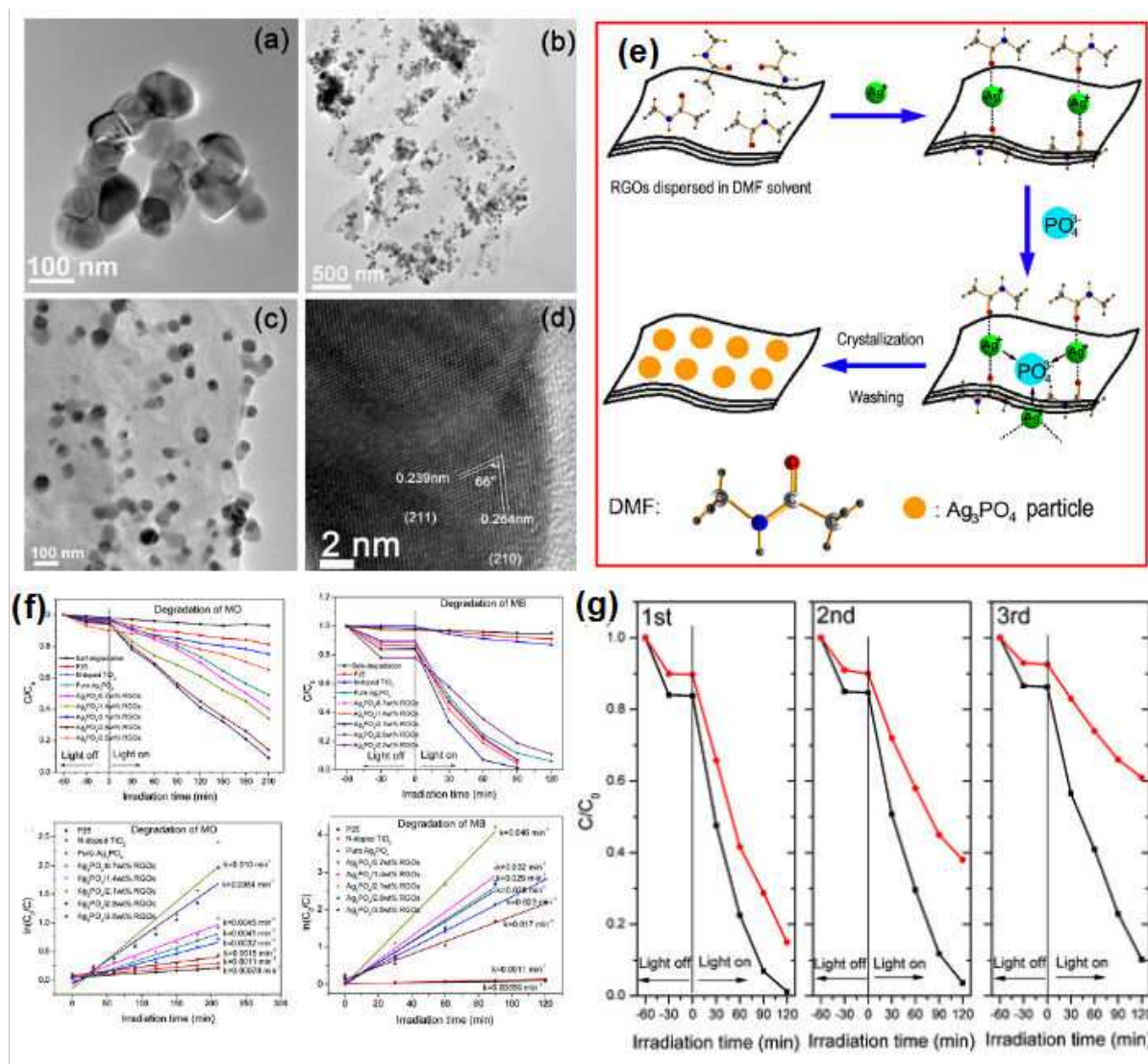
Figure 7. (a) TEM image of pure Ag_3PO_4 nanoparticles; (b and c) TEM images of Ag_3PO_4/2.1 wt% RGO nanocomposite; (d) HRTEM image of a single Ag_3PO_4 nanoparticle in the Ag_3PO_4/2.1 wt% RGO nanocomposite; (e) scheme of synthetic procedure for the Ag_3PO_4/RGO nanocomposite; (f) variation of MO and MB concentration against irradiation time using Ag_3PO_4/RGO nanocomposites with various RGO contents under visible-light irradiation and plots of $\ln(C_0/C)$ versus irradiation time representing the fit using a pseudo-first-order reaction rate; (g) repeated photocatalytic degradation of MB solution under visible-light irradiation. Reproduced with permission from ref. 134 © 2013 Elsevier B.V.

Ag_3PO_4/TiO_2 compounds under UV light irradiation, which is almost independent of self-corrosion. In contrast, it is the amount of visible-light response of Ag_3PO_4 in Ag_3PO_4/TiO_2 compounds that mainly determines the photocatalytic activities under visible-light irradiation, which is highly relevant to self-corrosion [146].

Besides Ag_3PO_4/TiO_2 composite heterostructures, AgX/Ag_3PO_4 (X = Cl, Br, I) heterocrystals have also attracted much attention due to their excellent photocatalytic activity [129]. Bi and coworkers have reported that the AgX/Ag_3PO_4 (X = Cl, Br, I) heterocrystals embodied some advantages compared to the single Ag_3PO_4, and it is a more promising and fascinating visible-
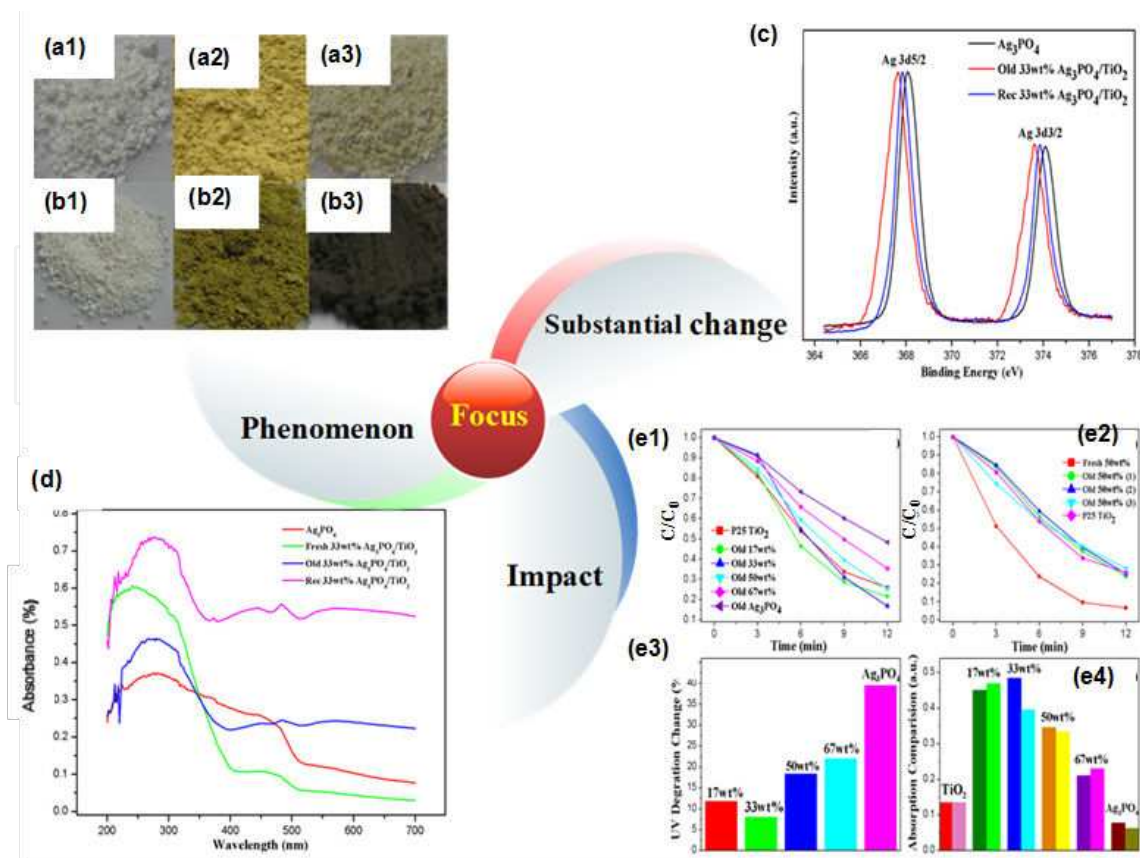
Figure 8. Images of fresh samples of (a1 and a3) P25 TiO_2, bare Ag_3PO_4, and Ag_3PO_4/TiO_2 compounds and their counterparts (b1 and b3) kept in dark for 5 days; (c) XPS spectra of Ag 3d; (d) UV–Vis absorption spectra for related samples; (e1) effects of "self-corrosion" on the photocatalytic activity under UV light irradiation, (e2) maintained time, (e3) decreased degradation percentage, (e4) adsorption capacity. Reproduced with permission from ref. 146 © 2014 Elsevier B.V.

light-driven photocatalyst than pure Ag_3PO_4 [129]. In their work, the $AgBr/Ag_3PO_4$ hybrid displayed much higher photocatalytic activity than single AgBr or Ag_3PO_4, as well as high stability under visible-light irradiation.

4. Long afterglow phosphor-assisted photocatalysts

Long afterglow phosphor-assisted novel photocatalysts become promising functional materials due to their effective utilization of solar light in practical applications of environmental purification. In this section, the recent development on TiO_2-based and Ag_3PO_4-based fluorescence photocatalyst composites with full-time active photocatalytic properties is reviewed.

The long afterglow phosphor ($CaAl_2O_4$:(Eu, Nd)) has a high luminescent brightness around 440 nm of wavelength, long afterglow time, good chemical stability, and low toxicity. The luminescent brightness around 440 nm can excite the visible-light-responsive nitrogen-doped titania ($TiO_{2-x}N_y$). Therefore, $TiO_{2-x}N_y$ photocatalyst was expected to possess a novel photocatalytic property after coupling with $CaAl_2O_4$:(Eu, Nd).

In our research [147–149], the degradation of continuous NO gas was achieved by $TiO_{2-x}N_y$ surface-immobilized $CaAl_2O_4$:(Eu, Nd) microparticles (Fig. 9). The results show a persistent deNOx ability of the $CaAl_2O_4$:(Eu, Nd)/$TiO_{2-x}N_y$ composite. In another work [149], the persistent fluorescence-assisted photocatalysts of Ag_3PO_4 composites have been synthesized to expand the application of Ag_3PO_4 on dye decomposition day and night. $Sr_4Al_{14}O_{25}$:(Eu,Dy)/Ag_3PO_4 composites exhibited excellent photocatalytic activities for the Rhodamine B (RhB) decomposition reaction in the dark without additional light sources (Fig. 9c).
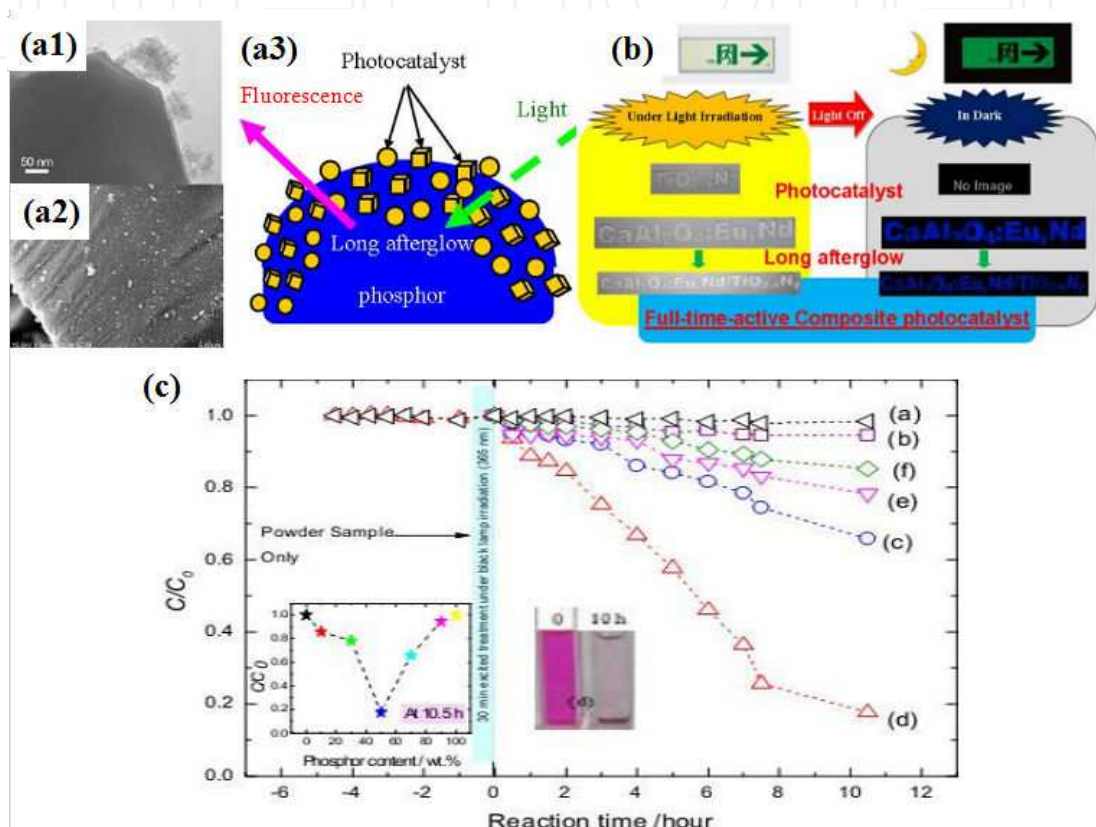

Figure 9. (a) Composition and (b) the mechanism of the persistent fluorescence-assisted photocatalysts; (c) variation of RhB solution concentration against illumination time using $Sr_4Al_{14}O_{25}$:(Eu,Dy)/Ag_3PO_4 composites. Reproduced with permission from ref. 148 © 2013 Elsevier B.V. & ref. 149 © 2013 RSC.

5. Challenges and perspectives

Photocatalysis appears to be a promising avenue to solve environmental and energy issues in the future. A variety of strategies, such as doping, coupling with graphene, precipitating with metal particles, crystal growth design, heterostructuring, were explored to enhance the efficiencies of photocatalytic activities. Besides modified TiO_2 and Ag_3PO_4, other visible-light-driven photocatalysts, including CdS, $BiVO_4$, Bi_2WO_6, and g-C_3N_4, even fluorescence-assisted photocatalyst composites, have attracted increased attention [147–156].

Although great progresses have been achieved, some challenges still exist to design high efficiency of photocatalytic systems. First, fundamental studies are essential to tackle the bottleneck problems in the field, including improved charge separation and transfer, promoted optical absorption, optimized band-gap position, lowered cost, and toxicity. Second, faceted photocatalysts remain a challenge and the development of surfactant-free synthesis routes is highly desirable, since most synthesis strategies involve the use of morphology-controlling agents that must be eventually removed in order to obtain clean facets. Finally, photostability of photocatalyst is and will continue to be a main challenge for practical applications. Therefore, new material design and innovative strategies for improving the efficiency and increasing the visible-light absorption of photocatalysts will be the key challenge and opportunity in this field.

Acknowledgements

Author details

Yuhua Wang[1,2*], Xinlong Ma[1,2], Hao Li[1,2], Bin Liu[1,2], Huihui Li[1,2], Shu Yin[3] and Tsugio Sato[3]

*Address all correspondence to: wyh@lzu.edu.cn

1 Key Laboratory for Special Function Materials and Structure Design of the Ministry of Education, Lanzhou University, Lanzhou, P. R. China

2 Department of Materials Science, School of Physical Science and Technology, Lanzhou University, Lanzhou, P. R. China

3 Institute of Multidisciplinary Research for Advanced Materials, Tohoku University, Aoba-ku, Sendai, Japan

References

[1]   A. Kudo and Y. Miseki, Chem. Soc. Rev., 2009, 38, 253–278.

[2]   M. Hoffmann, S. Martin, W. Choi and D. Bahnemann, Chem. Rev., 1995, 95, 69–96.

[3] Y. Hosogi, Y. Shimodaira, H. Kato, H. Kobayashi and A. Kudo, Chem. Mater., 2008, 20, 1299–1307.

[4] Z. Yi, J. Ye, T. Kako, S. Ouyang, H. Yang, W. Luo and R. Withers, Nat. Mater., 2010, 9, 559–564.

[5] L. Zhou, W. Wang, H. Xu, S. Sun and M. Shang, Chem. Eur. J., 2009, 15, 1776–1782.

[6] H. Cheng, B. Huang, X. Zhang and Y. Dai, Phys. Chem. Chem. Phys., 2010, 12, 15468–15475.

[7] J. Tang, Z. Zou and J. Ye, Angew. Chem. Int. Ed., 2004, 43, 4463–4466.

[8] F. Amano, A. Yamakata, M. Osawa and B. Ohtani, J. Am. Chem. Soc., 2008, 130, 17650–17651.

[9] L. Zhang, Y. Wang, H. Cheng, W. Yao and Y. Zhu, Adv. Mater., 2009, 21, 1286–1290.

[10] L. Zhang, H. Wang, Z. Chen, P. Wong and J. Liu, Appl. Catal. B:Environ., 2011, 106, 1–13.

[11] S. Yao, J. Wei, B. Huang, S. Feng, X. Zhang et al., J. Solid State Chem., 2009, 182, 236–239.

[12] A. Kudo, K. Omori and H. Kato, J. Am. Chem. Soc., 1999, 121, 11459–11467.

[13] G. Xi and J. Ye, Chem. Commun., 2010, 46, 1893–1895.

[14] R. Li, F. Zhang, D. Wang, J. Yang, M. Li, J. Zhu et al., Nat. Commun., 2013, 4, 1432.

[15] Y. Liu, B. Huang, Y. Dai, X. Zhang, X. Qin et al., Catal. Commun., 2009, 11, 210–213.

[16] Y. Liu, Z. Wang, B. Huang, X. Zhang, X. Qin et al., J. Colloid Interface Sci., 2010, 348, 211–215.

[17] W. Yao, X. Xu, H. Wang, J. Zhou, X. Yang et al., Appl. Catal. B:Environ., 2004, 52, 109–116.

[18] W. Wei, Y. Dai and B. Huang, J. Phys. Chem. C, 2009, 113, 5658–5663.

[19] H. Cheng, B. Huang, K. Yang, X. Y. Qin, Z. Wang et al., Chem. Phys. Chem., 2010, 11, 2167–2173.

[20] Y. Liu, Z. Wang, B. Huang, K. Yang, X. Zhang et al., Appl. Surf. Sci., 2010, 257, 172–175.

[21] W. Wang, B. Huang, X. Ma, Z. Wang, X. Qin et al., Chem. Eur. J., 2013, 19, 14777–14780.

[22] H. Cheng, B. Huang and Y. Dai, Nanoscale, 2014, 6, 2009–2026.

[23] W. Tu, Y. Zhou and Z. Zou, Adv. Funct. Mater., 2013, 23, 4996–5008.

[24] H. Chen, L. Shao, Q. Li, J. Wang and Chem. Soc. Rev., 2013, 42, 2679–2724.

[25] H. Tada, T. Kiyonaga and S. Naya, Chem. Soc. Rev., 2009, 38, 1849–1858.

[26] H. Tang, C. Hessel, J. Wang, H. Zhao and D. Wang, Chem. Soc. Rev., 2014, 43, 4281–4299.

[27] Q. Xiang, J. Yu and M. Jaroniec, Chem. Soc. Rev., 2012, 41, 782–796.

[28] K. Manga, Y. Zhou, Y. Yan and K. Loh, Adv. Funct. Mater., 2009, 19, 3638–3643.

[29] H. Li, Y. Zhou, W. Tu, J. Ye and Z. Zou, Adv. Funct. Mater. 2015, 25, 998–1013.

[30] J. Su, X. Zou, G. Li, Y. Wang, L. Zhou and J. Chen, J. Phys. Chem. C, 2011, 115, 8064–8071.

[31] X. Wang, Q. Xu, M. Li, H. Han and C. Li, Angew. Chem. Int. Ed., 2012, 51, 13089–13092.

[32] G. Liu, J. Yu, G. Lu and H. Cheng, Chem. Commun., 2011, 47, 6763–6783.

[33] R. Asahi, T. Morikawa, T. Ohwaki, K. Aoki and Y. Taga, Science, 2001, 293, 269.

[34] B. Liu, Y. Wang, Y. Huang, P. Dong and S. Yin, J. Austr. Ceram. Soc., 2012, 48, 249–252.

[35] S. Khan, M. Al-Shahry and W. Ingler, Science, 2002, 297, 2243.

[36] C. Di Valentin, G. Pacchioni and A. Selloni, Chem. Mater., 2005, 17, 6656–6665.

[37] S. Sakthivel and H. Kisch, Angew. Chem., Int. Ed., 2003, 42, 4908–4911.

[38] T. Umebayashi, T. Yamaki, H. Itoh and K. Asai, Appl. Phys. Lett., 2002, 81, 454–456.

[39] W. Ho, J. Yu and S. Lee, J. Solid State Chem., 2006, 179, 1171–1176.

[40] W. Zhao, W. Ma, C. Chen, J. Zhao and Z. Shuai, J. Am. Chem. Soc., 2004, 126, 4782–4783.

[41] G. Liu, Y. Zhao, C. Sun and H. Cheng, Angew. Chem., Int. Ed., 2008, 47, 4516–4520.

[42] S. In, A. Orlov, R. Berg, F. Garcia and R. Lambert, J. Am. Chem. Soc., 2007, 129, 13790–13791.

[43] J. Yu, J. Yu, W. Ho, Z. Jiang and L. Zhang, Chem. Mater., 2002, 14, 3808–3816.

[44] D. Li, H. Haneda and N. Labhsetwar, Chem. Phys. Lett., 2005, 401, 579–584.

[45] C. Di Valentin, E. Finazzi, M. Paganini and E. Giamello, Chem. Mater., 2008, 20, 3706–3714.

[46] H. Luo, T. Takata, Y. Lee, J. Zhao, K. Domen and Y. Yan, Chem. Mater., 2004, 16, 846–849.

[47] X. Hong, Z. Wang, W. Cai, F. Lu and J. Zhang, Chem. Mater., 2005, 17, 1548–1552.

[48] G. Liu, Z. Chen, C. Dong, G. Lu and H. Cheng, J. Phys. Chem. B, 2006, 110, 20823–20828.

[49] W. Su, Y. Zhang, Z. Li, L. Wu, X. Wang, J. Li and X. Fu, Langmuir, 2008, 24, 3422–3428.

[50] S. Tojo, T. Tachikawa, M. Fujitsuka and T. Majima, J. Phys. Chem. C, 2008, 112, 14948–14954.

[51] L. Lin, W. Lin, Y. Zhu, B. Zhao and Y. Xie, Chem. Lett., 2005, 34, 284–285.

[52] G. Liu, L. Wang, H. Yang, H. Cheng and G. Lu, J. Mater. Chem., 2010, 20, 831–843.

[53] G. Liu, C. Sun, L. Cheng, G. Lu and H. Cheng, J. Phys. Chem. C, 2009, 113, 12317–12324.

[54] J. Graciani, A. Nambu, J. Evans and J. Sanz, J. Am. Chem. Soc., 2008, 130, 12056–12063.

[55] T. Ikeda, T. Nomoto, K. Eda, A. Kudo and H. Onishi, J. Phys. Chem. C, 2008, 112, 1167–1173.

[56] V. Singh, D. Joung, L. Zhai, S. Khondaker and S. Seal, Prog. Mater Sci., 2011, 56, 1178–1271.

[57] H. Chae, D. Pérez, J. Kim, Y. Go, M. Eddaoudi et al., O. Yaghi, Nature, 2004, 427, 523–527.

[58] A. Geim and K. Novoselov, Nat. Mater., 2007, 6, 183–191.

[59] K. Loh, Q. Bao, P. Ang, J. Yang and J. Mater. Chem., 2010, 20, 2277–2289.

[60] Y. Liang, H. Wang, H. Casalongue, Z. Chen and H. Dai, Nano Res., 2010, 3, 701–705.

[61] Y. Zhang, Z. Tang, X. Fu and Y. Xu, ACS Nano., 2010, 4, 7303–7314.

[62] Y. Wang, R. Shi, J. Lin and Y. Zhu, Appl. Catal. B, 2010, 100, 179–183.

[63] X. Meng, D. Geng, J. Liu, R. Li and X. Sun, Nanotechnology, 2011, 22, 165602–165612.

[64] P. Wang, Y. Zhai, D. Wang and S. Dong, Nanoscale, 2011, 3, 1640–1645.

[65] J. Liu, H. Bai, Y. Wang, Z. Liu, X. Zhang and D. Sun, Adv. Funct. Mater., 2010, 20, 4175–4181

[66] J. Liu, L. Liu, H. Bai, Y. Wang and D. Sun, Appl. Catal. B:Environ., 2011, 106, 76–82.

[67] C. Wu, X. Huang, L. Xie, X. Wu, J. Yu and P. Jiang, J. Mater. Chem., 2011, 21, 17729–17736.

[68] B. Liu, Y. Huang, Y. Wen, L. Du, W. Zeng et al., J. Mater. Chem., 2012, 22, 7484–7491.

[69] P. Dong, Y. Wang, L. Guo, B. Liu, S. Xin et al., Nanoscale, 2012, 4, 4641–4649.

[70] H. Li, B. Liu, Y. Wang, Y. Shi, X. Ma et al., RSC Advance, 2014, 4, 37992–37997.

[71] H. Cheng, K. Fuku, Y. Kuwahara, K. Yamashita, J. Mater. Chem. A, 2015, 3, 5244–5258.

[72] X. Liu and M. T. Swihart, Chem. Soc. Rev., 2014, 43, 3908–3920.

[73] G. Baffou and R. Quidant, Chem. Soc. Rev., 2014, 43, 3898–3907.

[74] C. Clavero, Nat. Photonics, 2014, 8, 95–103.

[75] X. Chen, Z. Zheng, X. Ke, E. Jaatinen, T. Xie et al., Green Chem., 2010, 12, 414–419.

[76] S. Sun, W. Wang, L. Zhang, M. Shang and L. Wang, Catal. Commun., 2009, 11, 290–293.

[77] T. Takahashi, A. Kudo, S. Kuwabata, A. Ishikawa, H. Ishihara et al., J. Phys. Chem. C, 2013, 117, 2511–2520.

[78] X. Zhou, G. Liu, J. Yu and W. Fan, J. Mater. Chem., 2012, 22, 21337–21354.

[79] S. Kochuveedu, D. Kim and D. Kim, J. Phys. Chem. C, 2012, 116, 2500–2506.

[80] C. Li, Y. Zheng and T. Wang, J. Mater. Chem., 2012, 22, 13216–13222.

[81] M. Zhou, J. Zhang, B. Cheng and H. Yu, Int. J. Photoenergy, 2012, 2012, 532843.

[82] Y. Wen, B. Liu, W. Zeng and Y. Wang, Nanoscale, 2013, 5, 9739–9746.

[83] H. Tong, S. Ouyang, Y. Bi, N. Umezawa, J. Ye et al., Adv. Mater., 2012, 24, 229–251.

[84] X. Zhang, V. Thavasi, S. G. Mhaisalkar and S. Ramakrishna, Nanoscale, 2012, 4, 1707–1716.

[85] L. Huang, X. Wang, J. Yang, G. Liu, J. Han and C. Li, J. Phys. Chem. C, 2013, 117, 11584–11591.

[86] Z. Fang, Y. Liu, Y. Fan, Y. Ni, X. Wei et al., J. Phys. Chem. C, 2011, 115, 13968–13976.

[87] J. Jang, S. Choi, H. Kim and J. Lee, J. Phys. Chem. C, 2008, 112, 17200–17205.

[88] C. Li, J. Yuan, B. Han, L. Jiang and W. Shangguan, Int. J. Hydrogen. Energ., 2010, 35, 7073–7079.

[89] L. Sang, H. Tan, X. Zhang, Y. Wu, C. Ma and C. Burda, J. Phys. Chem. C, 2012, 116, 18633–18640.

[90] J. Ng, S. Xu, X. Zhang, H. Yang and D. Sun, Adv. Funct. Mater., 2010, 20, 4287–4294.

[91] H. Bai, Z. Liu and D. Sun, J. Am. Ceram. Soc., 2013, 96, 942–949.

[92] K. DeKrafft, C. Wang and W. Lin, Adv. Mater., 2012, 24, 2014–2018.

[93] X. Wang, G. Liu, G. Lu and H. Cheng, Int. J. Hydrogen. Energ., 2010, 35, 8199–8205.

[94] K. B. Chai, T. Peng, J. Mao and L. Zan, ACS Catal., 2013, 3, 170–177.

[95] J. Wang, H. Ruan, W. Li, D. Li, Y. Hu et al., J. Phys. Chem. C, 2012, 116, 13935–13943.

[96] X. Li, Y. Hou, Q. Zhao and G. Chen, Langmuir, 2011, 27, 3113–3120.

[97] A. Kezzim, N. Nasrallah, A. Abdi and M. Trari, Energ. Convers. Manag., 2011, 52, 2800–2806.

[98] Q. Simon, D. Barreca, A. Gasparotto, C. Maccato, T. Montini et al., J. Mater. Chem., 2012, 22, 11739–11747.

[99] Y. Liu, Y. X. Yu and W. D. Zhang, J. Phys. Chem. C, 2013, 117, 12949–12957.

[100] X. Zong, H. Yan, G. Wu, G. Ma, F. Wen et al., J. Am. Chem. Soc., 2008, 130, 7176–7177.

[101] D. Sarkar, C. Ghosh, S. Mukherjee and K. K. Chattopadhyay, ACS Appl. Mater. Interfaces, 2013, 5, 331–337.

[102] Y. Liao, H. Zhang, J. Zhang, L. Jia, F. Bai et al., ACS Appl. Mater. Interfaces, 2013, 5, 11022–11028.

[103] L. Lin, Y. Yang, L. Men, X. Wang, D. He et al., Nanoscale, 2013, 5, 588–593.

[104] Y. Hou, X. Li, Q. Zhao, X. Quan and G. Chen, Adv. Funct. Mater., 2010, 20, 2165–2174.

[105] Z. Zhang, C. Shao, X. Li, C. Wang, M. Zhang et al., ACS Appl. Mater. Interfaces, 2010, 2, 2915–2923.

[106] J. Yang, W. Liao and J. Wu, ACS Appl. Mater. Interfaces, 2013, 5, 7425–7431.

[107] L. Liau, Y. Lin and Y. Peng, J. Phys. Chem. C, 2013, 117 26426–26431.

[108] Y. Sun, W. Wang, L. Zhang and Z. Zhang, Chem. Eng. J., 2012, 211, 161–167.

[109] S. Chen, W. Liu, S. Zhang and Y. Chen, J. Sol–Gel Sci. Technol., 2010, 54, 258–267.

[110] F. Abdi, L. Han, A. Smets, M. Zeman, B. Dam and R. Krol, Nat. Commun., 2013, 4, 2195.

[111] Y. Qu, L. Liao, R. Cheng, Y. Wang, Y. Lin et al., Nano Lett., 2010, 10, 1941–1949.

[112] H. Yun, H. Lee, N. Kim, D. Lee, S. Yu and J. Yi, ACS Nano, 2011, 5, 4084–4090.

[113] H. Tada, T. Mitsui, T. Kiyonaga, T. Akita and K. Tanaka, Nat. Mater., 2006, 5, 782–786.

[114] X. Wang, L. Yin, G. Liu, L. Wang, R. Saito et al., Energy Environ. Sci., 2011, 4, 3976–3979.

[115] Z. Yu, Y. Xie, G. Liu, G. Lu, X. Ma and H. Cheng, J. Mater. Chem. A, 2013, 1, 2773–2776.

[116] S. Qin, F. Xin, Y. Liu, X. Yin and W. Ma, J. Colloid. Interf. Sci., 2011, 356, 257–261.

[117] M. Miyauchi, Y. Nukui, D. Atarashi and E. Sakai, ACS Appl. Mater. Interfaces, 2013, 5, 9770–9776.

[118] Y. Wang, Q. Wang, X. Zhan, F. Wang, M. Safdar and J. He, Nanoscale, 2013, 5, 8326–8339.

[119] T. Teranishi and M. Sakamoto, J. Phys. Chem. Lett., 2013, 4, 2867–2873.

[120] Y. Bi, S. Ouyang, N. Umezawa, J. Cao and J. Ye, J. Am. Chem. Soc., 2011, 133, 6490–6492.

[121] Y. Bi, H. Hu, Z. Jiao, H. Yu, G. Lu et al., Phys. Chem. Chem. Phys., 2012, 14, 14486–14488.

[122] W. Jun, F. Teng and M. Chen, CrystEngComm, 2013, 15, 39–42.

[123] Q. Liang, W. Ma, Y. Shi, Z. Li and X. Yang, CrystEngComm, 2012, 14, 2966–2973.

[124] Y. Bi, H. Hu, S. Ouyang, G. Lu, J. Cao and J. Ye, Chem. Commun., 2012, 48, 3748–3750.

[125] J. Liu, C. Luo, J. Wang, X. Yang and X. Zhong, CrystEngComm, 2012, 14, 8714–8721.

[126] H. Wang, L. He, L. Wang, P. Hu, L. Guo et al., CrystEngComm, 2012, 14, 8342–8344.

[127] S. Rawal, S. Sung and W. Lee, Catal. Commun., 2011, 17, 131–135.

[128] W. Yao, B. Zhang, C. Huang, C. Ma, X. Song and Q. Xu, J. Mater. Chem., 2012, 22, 4050–4055.

[129] Y. Bi, S. Ouyang, J. Cao and J. Ye, Phys. Chem. Chem. Phys., 2011, 13, 10071–10075.

[130] B. Cao, P. Dong, S. Cao and Y. Wang, J. Am. Ceram. Soc., 2013, 96, 544–548.

[131] G. Li and L. Mao, RSC Adv., 2012, 2, 5108–5111.

[132] L. Zhang, H. Zhang and H. Huang, New J. Chem., 2012, 36, 1541–1544.

[133] H. Zhang, H. Huang, H. Ming and L. Zhang, J. Mater. Chem., 2012, 22, 10501–10506.

[134] P. Dong, Y. Wang, B. Cao, S. Xin, L. Guo et al., Appl. Catal. B: Environ., 2013, 132–133, 45–53.

[135] Y. Liu, L. Fang, H. Lu, L. Liu, H. Wang and C. Hu, Catal. Commun., 2011, 17, 200–204.

[136] Y. Bi, H. Hu, S. Ouyang, Z. Jiao, G. Lu and J. Ye, J. Mater. Chem., 2012, 22, 14847–14850.

[137] Y. Liu, L. Fang, H. Lu, Y. Li, C. Hu et al., Appl. Catal. B: Environ., 2012, 115-116, 245–252.

[138] C. Haynes, A. McFarland and R. Duyne, Anal. Chem., 2005, 77, 338A–346A.

[139] B. Wiley, Z. Wang, J. Wei, Y. Yin, D. Cobden and Y. Xia, Nano Lett., 2006, 6, 2273–2278.

[140] M. Aslam, R. Bhobe, N. Alem, S. Donthu and V. Dravid, J. Appl. Phys., 2005, 98, 1–8.

[141] G. Somorjai and D. Blakely, Nature, 1975, 258, 580–583.

[142] D. Martin, N. Umezawa, X. Chen, J. Ye and J. Tang, Energy Environ. Sci., 2013, 6, 3380–3386.

[143] P. Dong, Y. Wang, H. Li, H. Li, X. Ma and L. Han, J. Mater. Chem. A, 2013, 1, 4651–4656.

[144] E. Bekyarova, M. Itkis, P. Ramesh, C. Berger, M. Sprinkle et al., J. Am. Chem. Soc., 2009, 131, 1336–1337.

[145] G. Williams, B. Seger and P.V. Kamat, ACS Nano, 2008, 2, 1487–1491.

[146] X. Ma, H. Li, Y. Wang, H. Li, B. Liu, et al., Appl. Catal. B: Environ., 2014, 158–159, 314–320.

[147] H. Li, S. Yin, Y. Wang, T. Sato, J. Catal., 2012, 286, 273–278.

[148] H. Li, S. Yin, Y. Wang, T. Sato, Appl. Catal. B:Environ., 2013, 132–133, 487–492.

[149] H. Li, S. Yin, Y. Wang, T. Sekino, S. Lee and T. Sato, J. Mater. Chem. A, 2013, 1, 1123–11261.

[150] J. Savio, A. Stephen, D. Martin, Z. Guo and J. Tang, Energy Environ. Sci., 2015, 8, 731–759.

[151] R. Li, H. Han, F. Zhang, D. Wang and C. Li, Energy Environ. Sci., 2014, 7, 1369–1376.

[152] T. Kim and K. Choi, Science, 2014, 343, 990.

[153] T. Saison, N. Chemin, C. Chanéac, O. Durupthy, V. Ruaux et al., J. Phys. Chem. C, 2011, 115, 5657–5666.

[154] Y. Huang, Z. Ai, W. Ho, M. Chen and S. Lee, J. Phys. Chem. C, 2010, 114, 6342–6349.

[155] Z. Zhao, Y. Sun and F. Dong, Nanoscale, 2015, 7, 15–37.

[156] C. Li, S. Wang, T. Wang, Y. Wei, P. Zhang and J. Gong, Small, 2014, 10, 2783–2790.